TRANSACTIONS OF THE INSTITUTE OF FLUID-FLOW MACHINERY

No. 135, 2017, 57–71

Jarosław Kaczyński* and Martin Kraft

Numerical investigation of particle separation in a centrifugal air separator

CTR Carinthian Tech Research AG, Europastrasse 12,
9524 Villach/St. Magdalen, Austria

Abstract

This paper presents the modeling approaches and results of numerical investigations into particle separation in a production-scale industrial centrifugal air separator. The gaseous phase was modeled using an Eulerian formulation, while the particle phase was modeled using a Lagrangian particle tracking approach. Two-way coupling between continuous and disperse phase was included and turbulence modeled using the realizable k-ε model. The resulting comprehensive system model provides correct predictions of the power consumption and of pressure losses in the device over the full operation range, and proved ability of accurately predicting the size-dependent particle separation efficiencies down to nominal particle sizes of 2 μm.

Keywords: CFD simulation; Discrete particle model; Particle separation

Nomenclature

A	–	area, m^2
C_D	–	drag coefficient
d	–	particle diameter, m
$\overline{d}$	–	characteristic (mean) diameter, m

*Corresponding author. E-mail address: jaroslaw.kaczynski@ctr.at

f	–	friction coefficient
F	–	force, $\mathrm{kg\,m\,s^{-2}}$
$\vec{g}$	–	gravitational acceleration, $\mathrm{ms^{-2}}$
k	–	coefficient of restitution
m	–	particle mass, kg
$\dot{m}$	–	mass flow rate, $\mathrm{kg\,s^{-1}}$
n	–	distribution parameter
p	–	pressure, $\mathrm{kg\,m^{-1}s^{-2}}$
Q	–	cumulative distribution function
$\vec{r}$	–	particle position vector
Re	–	Reynolds number
S	–	source term, $\mathrm{kg\,m^{-2}s^{-2}}$
t	–	time, s
$\vec{v}, u, v, w$	–	velocity, $\mathrm{m\,s^{-1}}$

Greek symbols

η	–	collection efficiency
μ	–	viscosity, $\mathrm{kg\,m^{-1}s^{-1}}$
ρ	–	density, $\mathrm{kg\,m^{-3}}$
Ψ	–	shape factor

Subscripts

D	–	drag
F	–	fluid (gas)
G	–	gravity
P	–	particle
t	–	turbulent
w	–	wall

1 Introduction

Disperse gas-particle or gas-droplet multiphase flows are common in mechanical, chemical and thermal process engineering. Consequently, a diverse range of processes and related equipment exists, ranging from conveying systems over particle size-dependent classification to fluid purification. Both the absolute size and the size distribution of particles or droplets are critical parameters for product quality and manufacturing process efficiency in many chemical, pharmaceutical and biological products, but also of importance, e.g., in modern 'clean' coal-fired power plants aiming at maximum efficiency.

At present, the design of processing equipment dealing with multiphase flows is largely limited to an experience plus tryout-based design process, though increasingly supported by computational fluid dynamics (CFD) simulations of the continuous fluid phase. This, however, is just an approximation of reality that

may be grossly inaccurate for some cases, e.g., the estimation of the power consumption of a particle classifier under load, and often neglects vital secondary phenomena, like an erosion by particle-wall interaction. The purpose of this work was hence to establish and validate a comprehensive multiphase CFD model capable of accurately simulating the complex processes in and the characteristic behaviour of a production-size industrial air classifier in one model. This model was then to be used for aiding the design process, but also for simulating the behaviour of the air separator at different operating points and its interaction with processes up- and downstream in the process chain.

1.1 Investigated system

The investigated example system was a Selex^{TM} 40 centrifugal air separator (OMYA AG) used for classifying submillimiter sized calcium carbonate particles in a continuous process. The system (see Fig. 1) comprises a cylindrical separator housing (1) with a tangential air inlet (2) and a coaxial charge inlet (3) for the material to be classified. The particles are classified by size during their passage through the louvre rotor (6) and leave the equipment either through the outlet for coarse material (4) into a discharge hopper, and are then typically returned to milling, or through the fines outlet (5) together with the air stream to be processed further.

The key element for the classification, i.e., the separation into finer and coarser particles, is the louvre rotor. Fine particles are carried through the rotor by the airflow, while coarser particles are prevented from following the fluid motion through the rotor lamellae into the inner space of the rotor cage by particle-wall interactions and are expelled into the outer housing. From this, they are – continuously or batch-wisely – discharged from the system.

The key parameters influencing the separation characteristics, i.e., the cut point and the collection efficiencies, are the design, the air flow and the rotor speed. In industrial practice, the latter is the parameter used to control the fineness of the output.

2 Numerical model description

The gas phase was modeled as a continuum, while the solid phase was modeled as discrete particles. A Lagrangian/Eulerian approach was applied to model the particle transport.

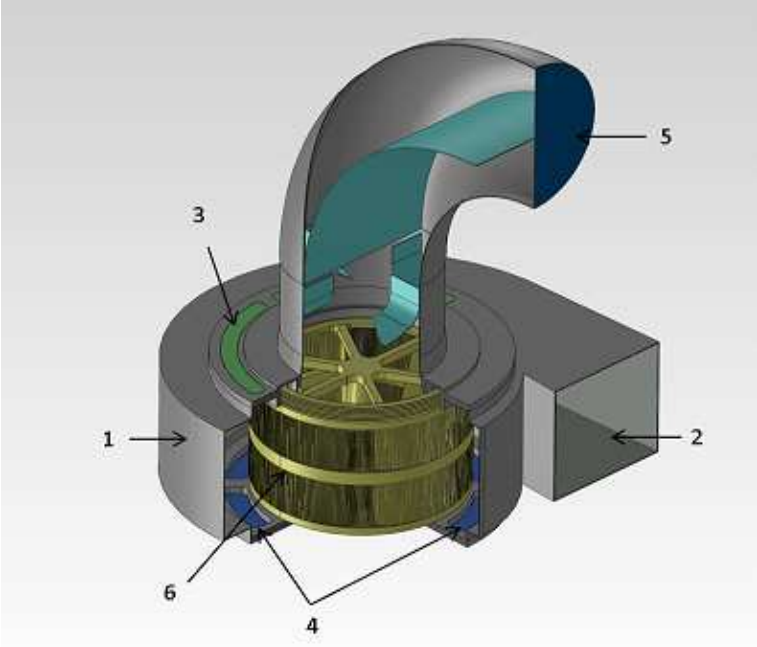

Figure 1: Basic system geometry of Selex^{TM} 40 centrifugal air separator:
1 – housing, 2 – air inlet, 3 – particle inlet, 4 – coarse matter outlet, 5 – fines & air outlet, 6 – louvre rotor.

2.1 Fluid motion modeling

The fluid phase was assumed to be: i) Newtonian, ii) have constant physical properties, and iii) in steady state. The fluid flow is thus assumed to be three-dimensional, incompressible, turbulent and isothermal. Fluid turbulence was modeled using the realizable k-ε model, neglecting (possible) influences of particle motion on fluid turbulence. Under these assumptions, all aspects of the time-averaged motion of the fluid phase can described by the general transport equation [1]

$$\frac{\partial}{\partial x_j}\left(\rho_F v_F^j \Phi\right) = \frac{\partial}{\partial x_j}\left(\Gamma \frac{\partial \Phi}{\partial x_j}\right) + S_F + S_P \,, \tag{1}$$

in which Φ is a general variable dependent on the parameter under consideration, Γ stands for the applicable diffusion coefficient, S_F for the respective source terms (s) and S_P describes the momentum exchange between the fluid and the particle phase using the particle-source-in cell (PSI-cell) method [2]. Table 1 provides an overview of the assignment to the concrete terms. The variables v_F^i

represent the fluid velocity components, k is the turbulent kinetic energy and ε the rate of dissipation of k. Index F indicates fluid, P indicates particle.

Table 1: Assignment of the general parameters in the general transport equation to the respective physical variables for calculating a specific parameter.

	Φ	Γ	S_F	S_P
Continuity	1	0	0	0
Momentum	v_F^i	$\mu + \mu_t$	$-\frac{\partial p}{\partial x_i} + \rho_F f_i$	$S_P^{v^i}$
Turbulent kinetic energy	k	$\mu + \frac{\mu_t}{\sigma_k}$	S_F^k	0
Dissipation of k	ε	$\mu + \frac{\mu_t}{\sigma_\varepsilon}$	S_F^ε	0

2.2 Disperse phase motion modeling

For adequately describing the disperse phase, the Lagrangian approach, i.e., the calculation of discrete particle trajectories, was chosen. The particle trajectories are predicted by solving the ordinary differential equations for the particle location and velocities.

The equations of motion for an individual particle can be written as follows:

$$\frac{d\vec{r}_P}{dt} = \vec{v}_P \tag{2}$$

and

$$m_p \frac{d\vec{v}_P}{dt} = \vec{F}_D + \vec{F}_G \tag{3}$$

with the drag force $\vec{F}_D$ described by

$$\vec{F}_D = C_D \frac{\pi}{8} \rho_F d_P^2 \left|\vec{v}_F - \vec{v}_P\right| \left(\vec{v}_F - \vec{v}_P\right) \tag{4}$$

and the gravity force $\vec{F}_G$ by

$$\vec{F}_G = \frac{\pi}{6} d_P^3 \left(\rho_P - \rho_F\right) \vec{g}\,. \tag{5}$$

Other contributions to the effective force acting on the particles, e.g., virtual mass or Basset force terms, were neglected because of the low fluid-to-particle density ratio of calcium carbonate particles ($\rho = 2700$ kg/m^3) in air.

The drag coefficient model for the – significantly nonspherical – particles was taken from the literature [3] as

$$C_D = \frac{a}{\mathrm{Re}_P} + \frac{b}{\sqrt{\mathrm{Re}_P}} + c \tag{6}$$

with the particle Reynolds number, Re_P, given by

$$\mathrm{Re}_P = \frac{\rho_F d_P v_{rel}}{\mu_F} \ ,$$

where v_{rel} is the absolute value of particle-fluid relative velocity, the factors a, b and c defined as functions of the shape factor Ψ

$$\begin{aligned} a &= 794.899\Psi^4 - 2294.985\Psi^3 + 2400.77\Psi^2 - 1090.0719\Psi + 211.686 \ , \\ b &= -320.575\Psi^4 + 933.336\Psi^3 - 973.461\Psi^2 + 433.488\Psi - 67 \ , \\ c &= 1/\left(22.265\Psi^4 - 35.241\Psi^3 + 20.365\Psi^2 4.131\Psi + 0.304\right) \ , \end{aligned}$$

with

$$\Psi = \frac{A_{SPH}}{A_P} \ ,$$

where A_{SPH} is the surface area of a sphere having an identical volume as the particle and A_P is the actual surface area of the particle.

2.3 Particle-wall interaction modeling

Like with the majority of industrially important disperse multiphase flows, the matter at hand deals with confined flows. Especially, the motion of larger particles, which is dominated by inertia, is strongly influenced by the confinement. The accurate description of the collision process of particles with solid walls is hence of high relevance, especially since it has been shown that irregularities due to the wall roughness and deviation of particle shapes from the ideal spherical form play an important role [4]. While the surface roughness is expected to play a minor role with the particle sizes of interest here, the pronounced nonsphericity of the mineral particles must not be neglected. In this study, the particle-wall collision was modelled using the sticking/sliding collision model [5]. Figure 2 shows the schematics of this particle-wall collision process.

For a particle colliding with a flat wall, two types of collision can be distinguished: collision with and without sliding. When neglecting angular velocity components, which is a reasonable assumption given the small size (≤ 0.1 mm)

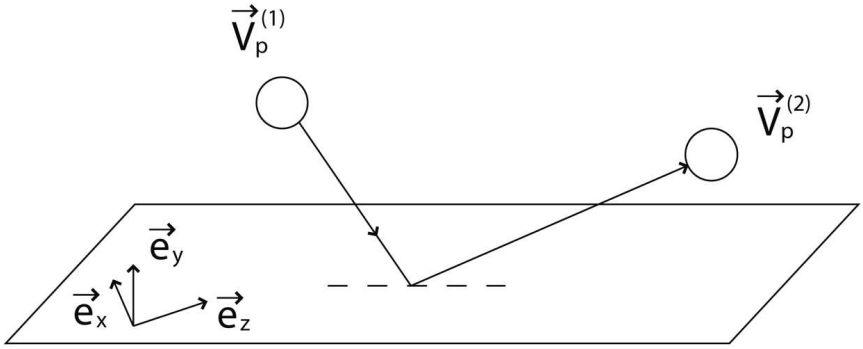

Figure 2: Schematics of the particle-wall collision process.

of the particles under consideration, both cases can be estimated using impulse equations [6]. For a collision involving sliding, i.e.,

$$-\frac{2}{7f_w\left(k_w+1\right)} \leq \frac{v_P^{(1)}}{|v_t|} \leq 0\,,$$

with

$$|v_t| = \sqrt{\left(u_P^{(1)}\right)^2 + \left(w_P^{(1)}\right)^2}\,,$$

$$\varepsilon_x = \frac{u_P^{(1)}}{|v_t|} \quad \text{and} \quad \varepsilon_z = \frac{w_P^{(1)}}{|v_t|}$$

the following applies

$$\begin{aligned} u_P^{(2)} &= u_P^{(1)} + \varepsilon_x f_w\left(k_w+1\right) v_P^{(1)}\,, \\ v_P^{(2)} &= -k_w v_P^{(1)}\,, \\ w_P^{(2)} &= w_P^{(1)} + \varepsilon_z f_w\left(k_w+1\right) v_P^{(1)}\,, \end{aligned} \tag{7}$$

while for a nonsliding collision, i.e.,

$$\frac{v_P^{(1)}}{|v_t|} < -\frac{2}{7f_w\left(k_w+1\right)}\,,$$

the terms are simplified to:

$$
\begin{aligned}
u_P^{(2)} &= \frac{5}{7} u_P^{(1)} \ , \\
v_P^{(2)} &= -k_w v_P^{(1)} \ , \\
w_P^{(2)} &= \frac{5}{7} w_P^{(1)} \ .
\end{aligned}
\tag{8}
$$

In Eqs. (7), and (8), k_w is the coefficient of restitution and f_w is the coefficient of kinetic friction. $|v_t|$ is the absolute value of tangential velocity of a colliding particle in the contact point. Superscripts (1) and (2) indicate values before and after collision, respectively.

The model was implemented in general-purpose CFD software [1] Fluent as user-defined functions (UDFs). In lieu of exact literature parameters for the mineral used in this process, data for a similar particle/wall material combination (limestone particles and a steel wall) was adopted from the literature [4]. The coefficient of restitution was thus set to $k_w = 0.5$, the coefficient of kinetic friction to $f_w = 0.45$, which should provide a good approximation of reality.

3 Simulation boundary conditions

All simulations were performed using Ansys Fluent CFD software [1]. Standard no-slip boundary conditions were applied to all walls, including the air separator impeller rotating at 2000 rpm. The model furthermore included two-way coupling between continuous and disperse phase.

The simulation geometry is a faithful representation of the factual design, except for minor details like welding seams and closed-off volumes that are of no practical relevance to the flows and were omitted to limit model complexity. Nevertheless, the geometry, and in particular the rotor comprising a large number of densely packed louvres, is highly complex. With the rotation of the rotor modeled using the multiple reference frames (MRF) option in the solver, the resulting hybrid grid consisted of 16×10^6 cells.

The standard operation point of the air separator was defined at an air flow rate of 40 000 m^3/h and a solid particle feed rate of 31 500 kg/h. The solid material is polydisperse calcium carbonate with a matter density of 2700 kg/m^3.

The discrete particle modeling (DPM) approach applied here initialises each particle trajectory by defining an initial position, velocity, size distribution and feed rate. The initial position is defined by the charge inlet (pos. 3 in Fig. 1), assuming a homogenous distribution of the particles across the inlet slits. The initial velocity is given by the flow rate of the charge makeup air flow, i.e., 1000 m^3/h, through the inlet slits, and the feed rate by overall solid particle feed rate and

the area of the particle inlet. To model the particle size distribution, the experimentally measured particle distribution in the charging material was fitted to the Rosin-Rammler equation [7]

$$Q_3(d) = 1 - e^{-\left(d/\bar{d}\right)^n}, \tag{9}$$

where $\overline{d}$ is the mean particle diameter, n is a spread parameter and Q_3 is the cumulative volume distribution function (Fig. 3). The fit curve used for the simulations thus has a mean diameter $\overline{d} = 21.39$ μm and a spread factor $n = 0.918$.

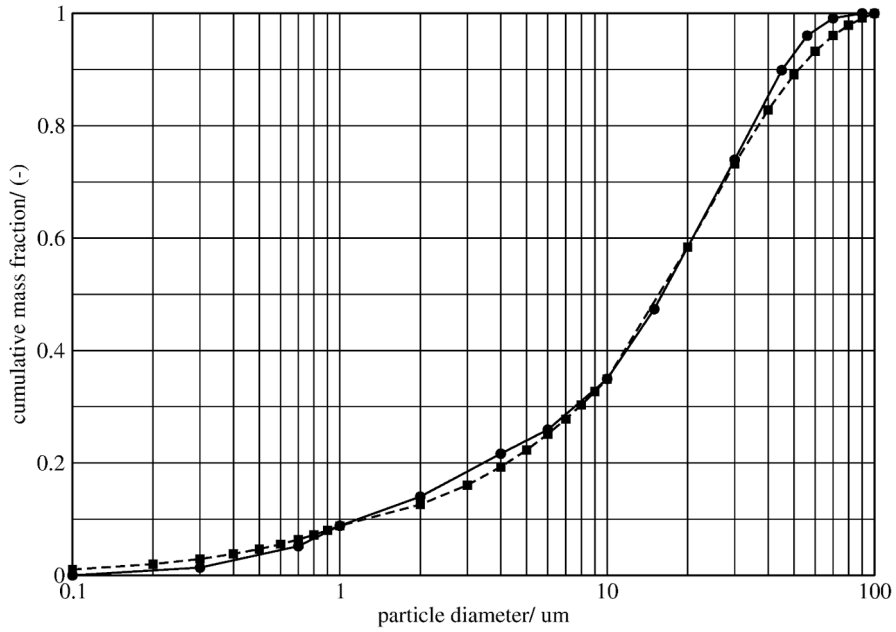

Figure 3: Experimentally determined particle size distribution (solid), overlaid with Rosin-Rammler distribution fit curve used for the simulation (dashed); circles represent measurement points, squares the particle classes and their populations as used in the simulation (semilogarithmic plot).

To achieve the required sensitivity of the simulation model over the entire wide range of interest, i.e., 0.1–100 μm with a reasonable number of particle classes, the range was subdivided into three ranges 0.1–1 μm, 1–10 μm, and 10–100 μm and 10 size classes assigned to each range. The full particle range spanning three orders of magnitude could thus be accurately modeled by just 28 classes.

4 Simulation results and validation

Given the highly experimental nature of the simulation approaches used in this work, the predictions of the models developed for describing the processes in and the resulting characteristics of the centrifugal air separator had to be validated. For this, a number of key reference parameters – in particular separation curves, power consumption of the rotor motor and pressures at different reference points – were measured on an Omya Selex^{TM} 40 operated at the given conditions.

4.1 Model development — key results

As outlined in the numerical model description section, the various submodels depend on various parameters, not all of which are precisely known or reliably derivable from known factors. The most prominent of these are the nonhericity of the particles, the wall-particle interaction parameters and the implementation of a reciprocal particle – fluid interaction.

Conducting a series of simulations with systematically varied parameters and comparison with the real-world data showed that: i) the two-way particle-fluid interaction does need to be taken into account, despite the higher complexity; ii) the wall interaction parameters taken from the literature for a similar case yield good results also for this application, and iii) the calcium carbonates as a collective are best characterised by a shape factor $\Psi = 0.6$.

4.2 System behaviour — gas flows

The motion of the gas phase clearly is the main driving factor influencing in the transportation of particles and thus the collection efficiency. Figure 4 shows typical contour plots of the gas velocities in the vertical central plan (Fig. 4a) and two horizontal planes (Fig. 4b). Figure 5 shows the corresponding contours of static pressure for the same visualisation planes. The predicted pressures both in the ring surrounding the rotor and in the elbow section leading to the fines outlet showed deviations of less than 8% to the measured values.

The final parameter used for validation is the power consumption under load. In this case, the predicted values were slightly less than 14% lower than the actual value measured at the electrical motor driving the rotor. The trend under different load conditions was accurately predicted by the simulation model. Given the fact that the simulation does obviously not take into account transmission losses in the mechanical and electrical system, this is a remarkably accurate forecast for a problem of that size and complexity.

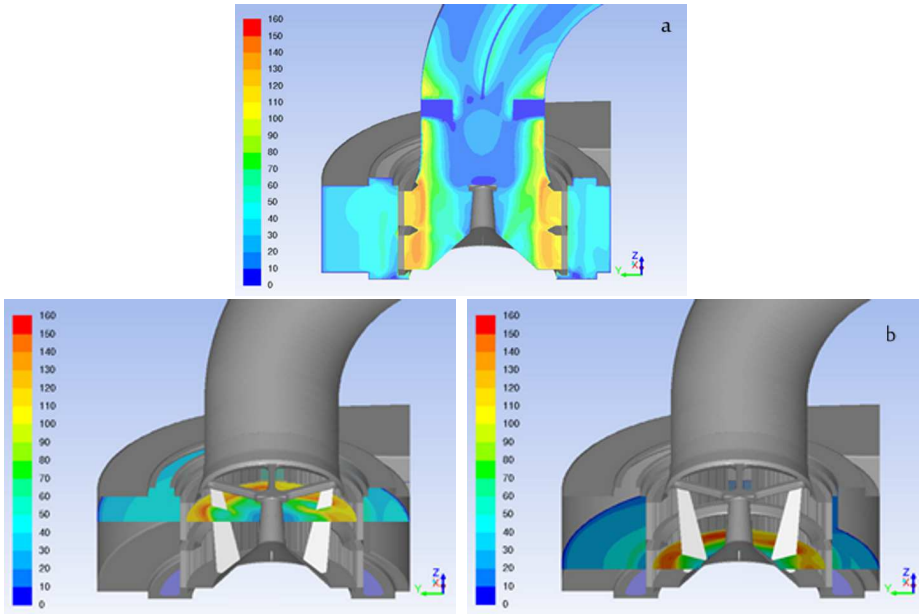

Figure 4: Contours of gas velocity in the air separator in m/s along the central vertical plane (a) and two horizontal planes (b).

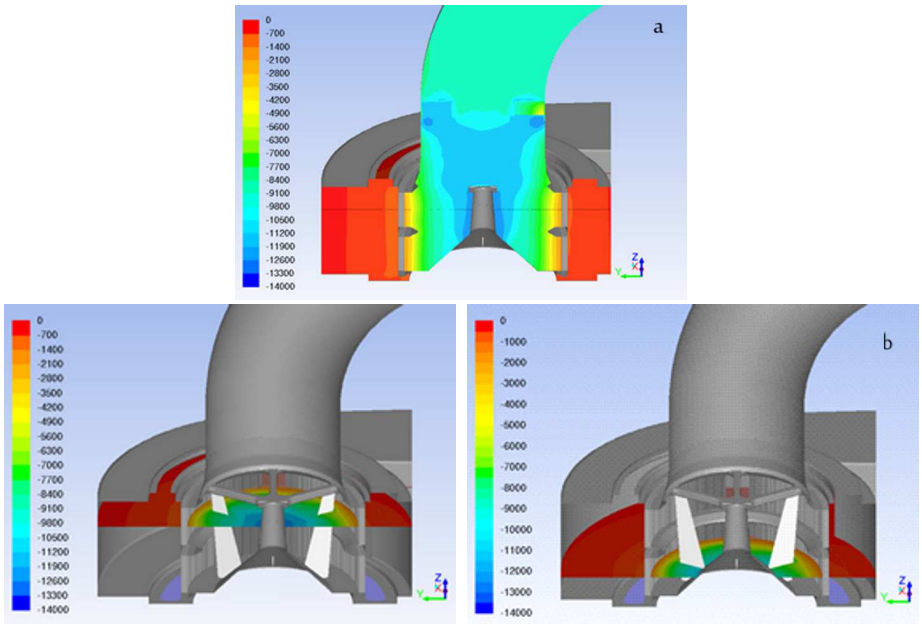

Figure 5: Contours of static pressure in Pa in the air separator along the central vertical plane (a) and two horizontal planes (b).

4.3 System behaviour – particle motion and collection efficiency

The key parameter of the air separator is the collection efficiency for particles of different sizes and thus the ability of the equipment to classify the particles by their size. Figure 6 shows the corresponding particle trajectories derived from the Lagrangian tracking for fine particles (nominal diameter 1 μm) well below and coarse particles (nominal diameter 50 μm) well above the desired 4 μm/50% collection efficiency cut level, $\eta(d)$, defined as

$$\eta\,(d) = 1 - \frac{\dot{m}_{out}\,(d)}{\dot{m}_{in}\,(d)}\,, \tag{10}$$

whereas $\dot{m}_{in}$ is the mass flow rate for a given particle size d in the inlet and $\dot{m}_{out}$ the mass flow rate for the same particle size in the gas outlet, i.e., the mass flow rate of the lightweight particles fraction.

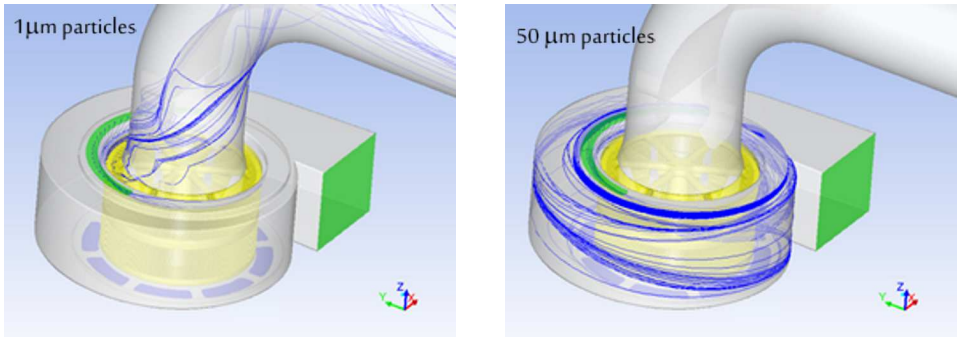

Figure 6: Typical trajectories of differently sized particles in the centrifugal air separator.

It is clearly evident that coarse particles, greater then 10 μm, are practically fully ($> 95\%$) retained in the outer housing, driven against the walls by the centrifugal forces of the rotor, while most of the small particles, lesser or equal to 1 μm follow the gas flow and escape the system through the fines outlet. Particles with nominal diameters $1 < d < 20$ μm can be found in both fractions, though in different amounts. The quantitative evaluation of this yields the characteristics shown in Fig. 7 in comparison to the actual, experimentally determined separation curve ('Tromp curve' [7]) of the device operated under identical conditions.

The comparison (Fig. 7) shows an excellent agreement between calculated and experimental values for particles with $d \geq 2$ μm, and increasingly strong deviations for submicrometer ultrafines. The same effect could be observed when simulating the same system with other operation parameters. The most probable

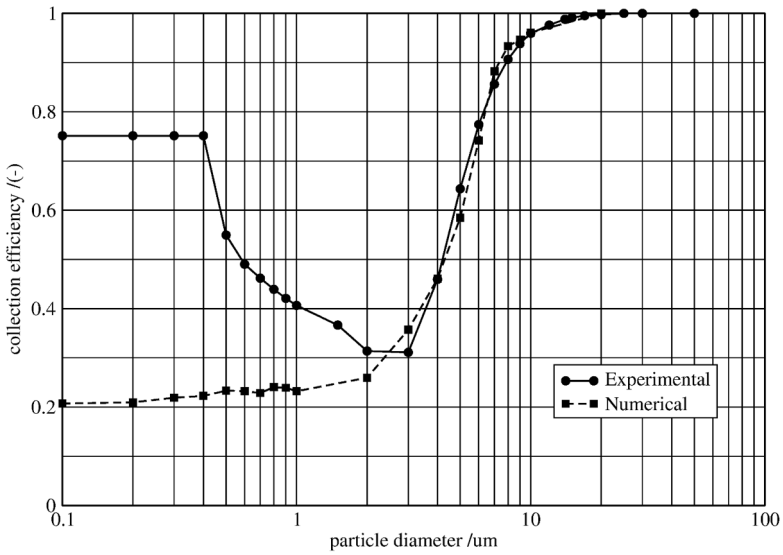

Figure 7: Comparison of experimentally measured (solid) and simulated (dashed) collection efficiencies *vs.* calculated separation efficiency $\eta(d)$.

reason for this diverging behaviour is that the Lagrangian approach used for the prediction of the particle motion does treat each particle as an independent entity that can follow the (turbulent) gas flow and collide with walls and other particles, but not stick to another particle (or a wall). In practice, however, the finer the particle, the higher it is the likelihood of its agglomeration with larger particles due to e.g. electrostatic forces. When stuck to larger particles, ultrafines are thus erroneously blown from the separator through the coarse particle outlet and only returned to their single particle state during particle size analysis, creating the effect observed here.

5 Conclusions

The results obtained by the numerical flow simulation in the centrifugal air separator prove that suitably designed CFD models are capable of efficiently and accurately simulating multiphase flows in the complex geometry plant. To ensure the quality and reliability of the simulation results, a deeper coverage of particle-

wall interactions, the effect of particle nonsphericity on the drag coefficient and the two-way coupling of the particles with the gas flow need to be taken into account.

The comparison of experimental results and simulation predictions yielded highly satisfactory agreement of pressure drops in and the power consumption of the system as a well the separation efficiency for different particle sizes. Significant deviations in the separation characteristics occur only with ultrafines, due to sticking effects beyond the prediction capability of CFD models. Following this validation, the numerical model was successfully used to systematically investigate the effects of both i) changes in the operating parameters, such as the inlet air conditions, the rotating speed of the rotor, the particle feed rate and the inlet particle size distribution, and ii) changes to the system geometry itself. CFD simulation thus proved its value as a system and process design tool even for such a complex, multiphase application as particle sizing in an industrial-scale centrifugal separator.

Acknowledgement We would like to thank OMYA AG, Gummern, Austria, for collaboration in this work and for providing the experimental results used for model validation. This work is part of the strategic research on comprehensive computer modeling of complex, integrated systems, performed within the Competence Centre *ASSIC – Austrian Smart Systems Research Center*, co-funded by the Austrian Federal Ministries of Transport, Innovation and Technology (bmvit) and Science, Research and Economy (bmwfw) and the Federal Provinces of Carinthia and Styria within the COMET – Competence Centers for Excellent Technologies Programme.

Received in March 2016

References

[1] ANSYS Inc, *ANSYS Fluent Theory Guide,* Fluent 12.0, 2009.

[2] Crowe C.T., Sharma M.P., Stock D.E.: *The particle-source-in cell (PSI-Cell) model for gas-droplet flows.* Trans. of ASME, J. Fluids Eng., **99**(1977), 2, 325–332.

[3] Salman A.D., Verba A.: *New approximate equations to estimate the drag coefficient of different particles of regular shape.* Periodica Polytechnica of the Technical University Budapest – Chem. Eng. **32**(1988), 4, 261–268.

[4] Frank T.: *Numerische Simulation der feststoffbeladenen Gasströmung im horizontalen Kanal unter Berücksichtigung von Wandrauhigkeiten.* PhD thesis, TU Bergakademie, Freiburg 1992.

[5] Tsuji Y., Oshima T., Morikawa Y.: *Numerical simulation of pneumatic conveying in a horizontal pipe*. KONA – Powder Sci. Technol. in Japan **3**(1985), 38–51.

[6] Sommerfeld M.: *Numerical simulation of the particle dispersion in turbulent flow: the importance of particle lift forces and particle wall collision models*. ASME Symp. on Numerical Methods for Multiphase Flows, Toronto 1990, 1–8.

[7] Farzanegan A., Ghomali M., Rahimyan M.H.: *Multiphase flow and Tromp curve simulation of dense medium cyclones using computational fluid dynamics*. J. Mining & Environment **4**(2013), 1, 67–76.